

The Fe–C system at 5 GPa and implications for Earth's core

Nancy L. Chabot^{a,*}, Andrew J. Campbell^b, William F. McDonough^b,
David S. Draper^c, Carl B. Agee^c, Munir Humayun^d, Heather C. Watson^e,
Elizabeth Cottrell^f, Sarah A. Saslow^g

^a Johns Hopkins University, Applied Physics Laboratory, 11100 Johns Hopkins Road, Laurel, MD 20723, USA

^b Department of Geology, University of Maryland, College Park, MD 20742, USA

^c Institute of Meteoritics, Department of Earth and Planetary Sciences, University of New Mexico, Albuquerque, NM 87131-1126, USA

^d National High Magnetic Field Laboratory and Department of Geological Sciences, Florida State University, Tallahassee, FL 32310, USA

^e Lawrence Livermore National Laboratory, 7000 East Avenue L-206, Livermore, CA 94550, USA

^f Department of Mineral Sciences, National Museum of Natural History, Smithsonian Institution, 10th & Constitution Avenue, Washington, DC 20560, USA

^g University of Maryland, College Park, MD 20742, USA

Received 26 December 2007; accepted in revised form 12 June 2008; available online 19 June 2008

Abstract

Earth's core may contain C, and it has been suggested that C in the core could stabilize the formation of a solid inner core composed of Fe₃C. We experimentally examined the Fe–C system at a pressure of 5 GPa and determined the Fe–C phase diagram at this pressure. In addition, we measured solid metal/liquid metal partition coefficients for 17 trace elements and examined the partitioning behavior between Fe₃C and liquid metal for 14 trace elements. Solid metal/liquid metal partition coefficients are similar to those found in one atmosphere studies, indicating that the effect of pressure to 5 GPa is negligible. All measured Fe₃C/liquid metal partition coefficients investigated are less than one, such that all trace elements prefer the C-rich liquid to Fe₃C. Fe₃C/liquid metal partition coefficients tend to decrease with decreasing atomic radii within a given period. Of particular interest, our 5 GPa Fe–C phase diagram does not show any evidence that the Fe–Fe₃C eutectic composition shifts to lower C contents with increasing pressure, which is central to the previous reasoning that the inner core may be composed of Fe₃C.

© 2008 Elsevier Ltd. All rights reserved.

1. INTRODUCTION

Between 5% and 10% of Earth's core is composed of elements lighter than Fe–Ni (e.g., Anderson and Isaak, 2002; McDonough, 2003). Considering the cosmochemical availability of elements, along with their atomic weights and ability to alloy with Fe–Ni, the elements H, C, O, Si, and S have been suggested as possible significant contributors to the light element component of Earth's core (e.g., Hillgren et al., 2000). The composition of the light elements

in Earth's core continues to be a major outstanding question in Earth science.

As our only samples of any cores, magmatic iron meteorites provide information about the light element composition of asteroidal cores (Scott, 1972). The presence of troilite, FeS, nodules in iron meteorites suggests S was present in asteroidal cores (Buchwald, 1975). Modeling the fractional crystallization of once completely molten metallic cores has had success at reproducing the elemental trends observed in magmatic iron meteorites when S is included as an important constituent of the asteroidal cores (e.g., Haack and Scott, 1993; Chabot, 2004). Of the proposed light elements, C is the second most abundant in the metallic phases in iron meteorites (Buchwald, 1975). Cohenite,

* Corresponding author. Fax: +1 240 228 8939.

E-mail address: Nancy.Chabot@JHUAPL.edu (N.L. Chabot).

$(\text{Fe},\text{Ni})_3\text{C}$, is found in iron meteorites, but the overall amount of C present in iron meteorites is much less than that of S.

However, there is a significant difference in pressure between an asteroid-sized body and an Earth-sized planet. This fact is important to consider before applying the results from iron meteorite studies to all planetary cores. Carbon is more cosmochemically abundant than S, but it is also more volatile, with the majority of carbon remaining in gaseous molecules, principally CO and CH_4 (Lodders, 2003). The volatile nature of C affects its behavior significantly during condensation from a solar gas. However, Wood (1993) pointed out that the volatility of C is strongly pressure dependent and that the pressures involved in planetary accretion and differentiation were substantially higher than during nebular condensation. Further, the pressure involved in such processes on an Earth-sized planet would be greater than that on an asteroid. In a combined theoretical and experimental study, Wood (1993) thus concluded that C should be a significant component of the light element content of Earth's core. We note, however, that if terrestrial planets formed from volatile-depleted precursors and not by devolatilization of a C-rich planet (Humayun and Clayton, 1995), then Wood (1993) would have overestimated the initial abundance of C available for such chemistry.

Additionally, the presence of C in planetary cores may significantly influence their evolution by affecting the first solid to crystallize. In his study, Wood (1993) advocated that Earth's solid inner core could be Fe_3C rather than solid Fe–Ni. Though Fe_3C is a subsolidus phase at 1 atm (Okamoto, 1990), at higher pressures, the Fe_3C stability field increases and Fe_3C can coexist with metallic liquid. The work of Wood (1993) suggested that at the high pressures applicable to planetary cores, the stability field of Fe_3C is large, such that any planetary core, even if it contained only 1 wt% C or less, would first solidify Fe_3C . Earth's inner core is perhaps slightly less dense than expected from solid Fe–Ni (e.g., Jepcoat and Olson, 1987) and Wood (1993) proposed that a solid inner core of Fe_3C could match the observed density deficit of Earth's solid inner core.

In reviewing current experimental constraints on the light element in Earth's core, Hillgren et al. (2000) concluded that the light element component of Earth's core was likely composed of multiple elements. The presence of other light elements, such as S, in addition to C could significantly affect the phase relations of the first solid to crystallize in the core; thus it was suggested that Earth's inner core could potentially be solid Fe–Ni even if C is a significant light element in the core (Hillgren et al., 2000). In contrast, Fei et al. (2008) have begun to experimentally explore the phase relations in the Fe–S–C system and their preliminary work suggests that in this system, depending on the pressure and the $\text{Fe}/(\text{S} + \text{C})$ ratio, the first solid to form may be an iron carbide, not solid Fe.

Using synchrotron-based X-ray diffraction, Scott et al. (2001) measured the volume and lattice parameters of Fe_3C at pressures up to 73 GPa. The results of Scott et al. (2001) were in close agreement with the values used in the study of Wood (1993), though Scott et al. (2001) cautioned that they considered it premature to extrapolate

their results to Earth's inner core conditions. Scott et al. (2001) did conclude that C could be a major light element in Earth's core. Similarly, Li et al. (2002) determined equation-of-state parameters for Fe_3C up to 30.5 GPa, which were in good agreement with both the Scott et al. (2001) study and the values used in the Wood (1993) work. Li et al. (2002) also cautiously stated that the experimental pressures were far from those experienced in Earth's core and that the effect of temperature was barely known.

Partially motivated by the Scott et al. (2001) and Li et al. (2002) results, Vocadlo et al. (2002) used first-principle calculations to examine the equation of state of Fe_3C as applied to Earth's core. Vocadlo et al. (2002) concluded that at the high pressures and temperatures applicable to Earth's core, Fe_3C has no magnetic ordering and the calculated density and incompressibility for Fe_3C was significantly different from that observed by seismic studies of Earth's inner core. Vocadlo et al. (2002) thus concluded that Fe_3C was not a major component of Earth's inner core. Work by Wood et al. (2004) using high-resolution neutron powder diffraction determined that the thermal expansion of Fe_3C is dependent on temperature, supporting the study of Vocadlo et al. (2002), and stressed the importance of using values appropriate to a high-temperature, high-pressure phase of Fe_3C when modeling Earth's core.

Therefore, while there is reason to suspect the presence of C as a component of Earth's core, its potential effect on phase equilibria remains under debate. In this study, we experimentally examine the Fe–C system at 5 GPa. Our experiments allow us to map out the Fe–C phase diagram and compare our results directly to the predicted 5 GPa Fe–C phase diagram published in Wood (1993). Although we cannot attain the pressures relevant to Earth's inner core–outer core equilibrium (330 GPa), we can determine if the Fe– Fe_3C eutectic trends in the right direction with increasing pressure to allow the possibility of Fe_3C in Earth's core. With these same experiments, we can also compare our 5 GPa solid metal/liquid metal partitioning results to those obtained at 1 atm (Chabot et al., 2006) to examine the effect of pressure on partitioning behavior. In addition, our experiments yield the partitioning behavior of trace elements between Fe_3C and liquid metal to explore the types of fractionations that may be generated if planetary cores contain Fe_3C .

2. METHODS

All experiments were conducted at the University of New Mexico in a multi-anvil press at a pressure of 5 GPa. Tungsten-carbide cubes with a truncated edge length of 8 mm were used to generate the pressure, and experiments were conducted using castable octahedral assemblies similar to that described in Agee et al. (1995). The run temperatures ranged from 1200 to 1600 °C, and the temperature was measured throughout the experiment with a $\text{W}_{97}\text{Re}_3/\text{W}_{75}\text{Re}_{25}$ thermocouple placed axially through the assembly. A Re foil furnace was used to heat the experiments.

Starting powders of Fe, Ni, and C were contained in alumina capsules. Trace elements of Ag, As, Au, Bi, Co, Cu, Ga, Ge, Ir, Mo, Os, Pb, Pd, Pt, Re, Ru, Sb, and W were

added to the starting mixtures at concentrations of a few hundred ppm each. Run durations varied between 30 min to just over 6 h. At a temperature of 1250 °C, a time series consisting of four experiments was conducted. The results of the time series are shown in detail in the next section, but the series showed that equilibrium partitioning behavior was achieved for all of the elements studied in a time of less than 30 min.

Initially, our experimental approach involved raising all experiments to a temperature of 1600 °C for a duration of 5 min and then lowering the temperature to the desired run temperature. The motivation for this approach was to raise the starting composition above the liquidus temperature, which could potentially assist with reaching trace element partitioning equilibrium in the experiments and with growing large solid phases in the run products. In actuality, this step greatly complicated our interpretation of the run products. As shown in Fig. 1, a C-bearing metallic liquid can quench to a wide range of textures. Because the quenched C-bearing metallic liquids looked so different with only slight differences in composition or temperature, it was difficult to confidently examine a run product's texture and distinguish between whether the run had been completely liquid at run conditions or whether solids had formed quickly from a liquid cooled from 1600 °C to the final run temperature. However, distinguishing between these two options was crucial to our study and to understanding the Fe–C phase diagram at 5 GPa. Consequently,

we eliminated the step of raising all experiments to 1600 °C in our later experiments (all experiments with run numbers of the form A4XX). To verify that we were still creating the same phases, we conducted an experiment (A416) which was a duplicate of the experiments used in the time series, all of which had been raised to 1600 °C, but that was raised straight to the desired run temperature of 1250 °C; experiment A416 produced the same solid metal and liquid metal phases observed in the time series set. Thus, with this convergent experiment and with the results of our time series, we feel confident in the equilibrium partitioning values we report and in the phase identifications for each of our reported runs.

Runs were first inspected via back-scattered electron images at the University of New Mexico using a JEOL 8200 electron microprobe, as shown in Fig. 1. The major elements of Fe and C (and Ni in Run #A177) were analyzed using the JEOL 8900L electron microprobe at the Carnegie Institution of Washington. Probe conditions of 15 kV accelerating voltage, 30 nA beam current, and 30 s. counting time were used for all analyses, as was a 10 μm × 10 μm raster beam. Multiple analysis points were averaged to determine the major element composition of each phase. Fe was analyzed using a LIFH crystal, Ni using a LIF crystal, and C using a LDE2 crystal.

As discussed by Wood (1993), C can be analyzed on the probe but special precautions must be taken. First, C-coating samples, as commonly done for microprobe analysis,

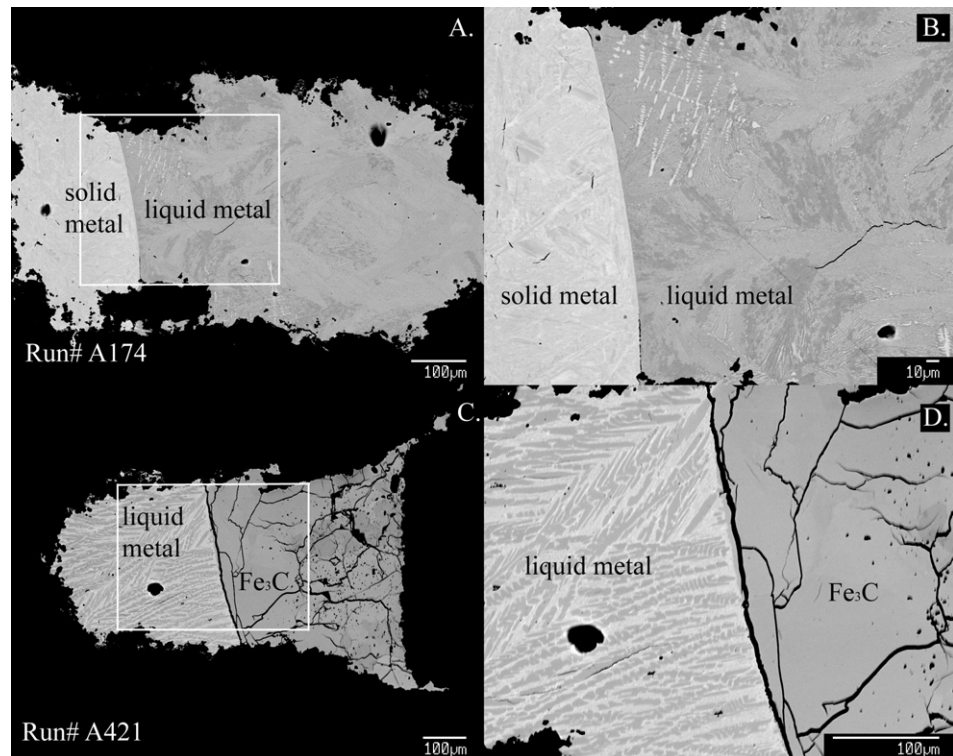


Fig. 1. Back-scattered electron (BSE) images of two experimental run products are shown. (A) Run #A174 produced coexisting solid metal and C-bearing liquid metal. (B) A magnified view of #A174 shows the quench texture of the metallic liquid. (C) Run #A421 contained C-bearing liquid metal and Fe₃C. (D) The C content of Fe₃C is higher than that of the liquid metal, consistent with its darker appearance in the BSE images. The liquid metal did not quench to a single phase but rather formed an intergrowth of Fe₃C and C-bearing Fe phases.

can complicate the accurate measurement of C in the experimental samples. For our analysis, we did not C-coat our samples but rather used C paint to overlap with the run product and allow charge transfer during the analysis. Because the samples were metallic in nature, a coating on the actual phases measured in the run products could be avoided.

Second, reliable C standards are difficult to find. Our first attempts used NIST steels as standards. However, upon inspection, the NIST steels were found to be compositionally heterogeneous on scales of 100 or more microns; for our analysis, which used a 10- μm raster beam, different analysis points on the NIST steels yielded different compositions. Thus, we decided to use the Fe₃C formed in our Run #A421, shown in Fig. 1, as our C standard. By defining the Fe₃C in this run to have 6.7 wt% C, we were able to measure the C contents of the other runs. Pure metals of Fe and Ni were used as standards, and, similar to the samples, the standards were not C-coated.

Third, there is generally a background contribution to the measured C content of a sample. As noted by Wood (1993) and similarly observed by us, if a sample is repeatedly measured for C using the electron microprobe, the measured C content will increase as the measurement time increases. This is attributed to C being deposited on the sample from C present in the probe during analysis. Our attempt to utilize a cold trap to eliminate any C deposition on the sample did nothing to change the observed increase in C with measurement time. To monitor this contribution, we repeatedly analyzed a new, previously unanalyzed, portion of the pure Fe metal standard throughout our microprobe analysis using identical analytical conditions to those used for our C-bearing experimental samples. This C-free sample was measured to consistently have 0.8 wt% C. No attempt was made to correct for this background contribution, meaning our reported C concentrations may be slightly high. However, we did define the Fe₃C in Run #A421 to have 6.7 wt% C, which accounts for the C from the background and from the Fe₃C in the sample.

As an additional precaution, all samples were analyzed for Fe, Ni, and C during the same 24-h probe session. Throughout this session, the pure Fe standard and the defined #A421 Fe₃C standard were regularly analyzed to confirm the repeatability of the measurements. Thus, our reported C measurements may be slightly high due to the background C contribution, but our dataset for reported relative C contents is self-consistent. Furthermore, Runs #A424 and #A425 produced run products that were all liquid; the measured C composition of the resulting liquid should thus be that of the starting bulk composition. Run #A424 had a starting composition of 6 wt% C, and the measured liquid composition was 5.7 ± 0.3 wt% C; Run #A425 began with a bulk composition of 2 wt% C, and the measured liquid composition was 2.1 ± 0.7 wt% C. This agreement provides additional confidence in our C measurements.

The Fe₃C in Run #A421 was used as a defined standard for C, but the C content of the Fe₃C phases in Runs #A417 and #A423 were determined independently. The measured C content of the Fe₃C phase in Run #A417 was

6.8 ± 0.4 wt%, a value entirely consistent with the expected Fe₃C composition of 6.7 wt% C. For Run #A423, measurements of the Fe₃C repeatedly yielded higher than expected C concentrations, with a composition of 7.8 ± 0.2 wt% C. We do not have an explanation for this high C content, but we also appreciate that this value, though slightly high, may be a result of the limited accuracy with which we can make these C measurements, given our analytical techniques.

Trace elements for the solid metal/liquid metal time series experiments were analyzed by laser ablation inductively coupled plasma mass spectrometry (ICP-MS) at the University of Chicago. Laser ablation ICP-MS analyses were performed using a CETAC LSX-200 laser ablation peripheral with a magnetic sector ICP mass spectrometer, the Finnigan Element™, using techniques similar to those described by Campbell and Humayun (1999b), Campbell et al. (2002), and Chabot et al. (2003). Measurements were made using laser ablation points that were 50 μm in diameter and by averaging six points for each phase analyzed. During the analyses, the mass spectrometer was swept repeatedly over the mass range of interest, once per 0.8 s, and counts were accumulated at selected masses. To maximize signal to noise ratios and to avoid overlap with isotopes of neighboring elements or background sources, the following isotopes were measured during analysis: ⁵⁷Fe, ⁵⁹Co, ⁶⁰Ni, ⁶³Cu, ⁶⁹Ga, ⁷⁴Ge, ⁷⁵As, ⁹⁵Mo, ¹⁰¹Ru, ¹⁰⁵Pd, ¹⁰⁷Ag, ¹²¹Sb, ¹⁸²W, ¹⁸⁵Re, ¹⁹²Os, ¹⁹³Ir, ¹⁹⁵Pt, ¹⁹⁷Au, ²⁰⁸Pb, and ²⁰⁹Bi. The concentration of Re in these solid metal/liquid metal samples was found to be slightly high and variable between measurement points, perhaps due to contamination of the sample from the Re furnace, and Re compositions were consequently not considered reliable indications of equilibrium behavior for these solid metal/liquid metal experiments. Background subtractions were performed using the average of three blank measurements that were run either immediately before or after each set of analyses. Instrumental sensitivity factors for each isotope relative to ⁵⁷Fe were determined by measuring the signal intensity from the known standards of Hoba and NIST SRM 1263a (Campbell et al., 2002). The corrected intensities were normalized to 100%, taking into account the amount of Fe, Ni, and C in the solid metal and liquid metal phases as determined by the electron microprobe analysis results.

Trace elements for the Fe₃C/liquid metal experiments were conducted at the University of Maryland by laser ablation ICP-MS. The use of two different analytical laser ablation ICP-MS facilities came about as a result of many of the authors transitioning to new home institutions during the duration of this project. However, Chabot et al. (2007) demonstrated that there is good agreement between the measurements conducted at both facilities. In-situ analyses were carried out using a single-collector ICP-MS (Element 2, Thermo Electron Corp) coupled to a laser ablation system with an output wavelength at 213 nm (UP213, New Wave Research). The laser was operated with a uniform energy density of ~ 2.6 J/cm². Ablation sampling was done in line scan mode using a 30- μm diameter spot and 7 Hz flash rate. The sample was moved at a rate of 10 $\mu\text{m}/\text{s}$ during ablation. The lengths of the line scans

varied depending on the specific features of each run product but were generally 100 µm in length. Four line scans were conducted in each Fe₃C and liquid metal phase. Data were collected for the following masses: ⁵⁷Fe, ⁵⁹Co, ⁶³Cu, ⁶⁵Cu, ⁶⁹Ga, ⁷¹Ga, ⁷⁵As, ⁹⁵Mo, ⁹⁷Mo, ⁹⁹Ru, ¹⁰¹Ru, ¹⁰⁵Pd, ¹⁰⁷Ag, ¹⁰⁸Pd, ¹⁰⁹Ag, ¹⁸²W, ¹⁸³W, ¹⁸⁵Re, ¹⁸⁸Os, ¹⁸⁹Os, ¹⁹¹Ir, ¹⁹³Ir, ¹⁹⁴Pt, ¹⁹⁵Pt, and ¹⁹⁷Au. In contrast to the solid metal/liquid metal runs, the concentration of Re was not observed to be variable in these Fe₃C/liquid metal samples, and consequently measured Re compositions were considered reliable for these experiments. Analyses of Fe₃C and liquid metal pairs were accompanied by the analyses of two standard reference materials (Filomena and SRM NIST 610) before and after the sample acquisition, which provided the calibration curves for determining element concentrations and for constraining instrument drift. Data were processed using the LAMTRACE (Achterbergh et al., 2001) software program, which determines element concentrations based on ratios of count rates for samples and standards, known concentrations in the standards, and the known concentration of an internal standard in the unknowns.

3. RESULTS AND IMPLICATIONS

3.1. Fe–C phase diagram at 5 GPa

The phases present in each experiment along with their major element compositions are given in Table 1. Errors

are twice the standard deviation of the mean of multiple probe measurements. Two experiments were conducted at 1200 °C with different starting bulk compositions, one with 3 wt% C and one with 6 wt% C. Both experiments were found to be subsolidus and produced experiments with coexisting Fe₃C and solid metal; the relative amounts of Fe₃C and solid metal were different in the two experiments, due to the different bulk compositions, but the compositions of the resulting phases were consistent between the two experiments.

Five experiments were conducted at 1250 °C with a starting composition of 3 wt% C. All five experiments produced two coexisting phases of solid metal and liquid metal, as shown for Run #A174 in Fig. 1. Run #A177 of these five experiments also contained about 10 wt% Ni, and the similar phases produced in #A177 as compared to the other four runs at 1250 °C suggests that the presence of 10 wt% Ni does not have a significant effect on the phase relations for this portion of the phase diagram.

Three runs were conducted with a starting composition of 2 wt% C at temperatures of 1300, 1450, and 1600 °C. The experiments at 1300 °C (#A167) and 1450 °C (#A420) produced run products with both solid metal and liquid metal, while the run at 1600 °C (#A425) contained just a single C-bearing liquid.

Four experiments were conducted above the solidus with a starting composition of 6 wt% C. The experiments at 1300 and 1350 °C yielded run products that contained coexisting

Table 1
Experimental run conditions at 5 GPa and resulting phases

Run #	Temperature (°C)	Duration (min)	Phase ^a	Fe (wt%)	Ni (wt%)	C (wt%)	Total
A418	1200	90	SM	100.1 ± 0.9		1.5 ± 0.1	101.6 ± 0.9
A418	1200	90	Fe ₃ C	93.8 ± 1.2		6.1 ± 0.8	99.9 ± 1.4
A422	1200	77	SM	99.5 ± 0.5		1.7 ± 0.1	101.2 ± 0.5
A422	1200	77	Fe ₃ C	94.3 ± 1.3		6.0 ± 0.4	100.3 ± 1.4
A174	1250	30	SM	97.0 ± 0.6		2.3 ± 0.2	99.3 ± 0.6
A174	1250	30	LM	94.6 ± 1.5		4.6 ± 0.2	99.2 ± 1.5
A416	1250	38	SM	99.6 ± 1.1		1.7 ± 0.1	101.3 ± 1.1
A416	1250	38	LM	96.9 ± 0.7		4.3 ± 0.2	101.2 ± 0.7
A168	1250	121	SM	99.0 ± 1.1		2.0 ± 0.1	101 ± 1.1
A168	1250	121	LM	97.0 ± 0.7		4.5 ± 0.4	101.5 ± 0.8
A177	1250	197	SM	86.0 ± 0.1	14.1 ± 0.3	1.8 ± 0.1	101.9 ± 0.3
A177	1250	197	LM	87.3 ± 0.5	9.9 ± 0.2	4.3 ± 0.2	101.5 ± 0.6
A176	1250	375	SM	97.4 ± 1.6		1.7 ± 0.1	99.1 ± 1.6
A176	1250	375	LM	96.4 ± 1.5		3.8 ± 0.4	100.2 ± 1.6
A167	1300	151	SM	96.9 ± 1.4		1.6 ± 0.1	98.5 ± 1.4
A167	1300	151	LM	n.d.		3.9 ± 0.5	n.d.
A417	1300	95	Fe ₃ C	92.8 ± 0.5		6.8 ± 0.4	99.6 ± 0.6
A417	1300	95	LM	95.3 ± 0.8		4.9 ± 0.6	100.2 ± 1.0
A421	1350	37	Fe ₃ C	93.7 ± 1.2		6.9 ± 0.7	100.6 ± 1.4
A421	1350	37	LM	94.1 ± 1.4		5.8 ± 0.8	99.9 ± 1.6
A423	1350	181	Fe ₃ C	94.1 ± 0.7		7.8 ± 0.2	101.9 ± 0.7
A423	1350	181	LM	95.9 ± 0.7		5.3 ± 0.8	101.2 ± 1.1
A424	1400	49	LM	94.3 ± 1.0		5.7 ± 0.3	100 ± 1.0
A420	1450	35	SM	100.0 ± 0.9		1.4 ± 0.1	101.4 ± 0.9
A420	1450	35	LM	98.0 ± 1.1		3.5 ± 0.9	101.5 ± 1.4
A425	1600	48	LM	n.d.		2.1 ± 0.7	n.d.

n.d., the Fe content was not determined during the measurements.

Errors are twice the standard deviation of the mean.

^a Phase abbreviations: SM, solid metal; LM, liquid metal.

Fe_3C and liquid metal, as shown for Run #A421 in Fig. 1. The liquid metal was a homogenous liquid at run conditions but formed a texture composed of Fe_3C and dominantly Fe metal during quenching of the experiment. An experiment with a bulk composition of 6 wt% C conducted at 1400 °C (#A424) produced a run product with a single metallic liquid.

The phases produced in our 5 GPa experiments differ from those predicted by the 1 atm phase diagram (Okamoto, 1990), which is not surprising due to the difference in pressure. Fig. 2A shows the phase information from our experiments overlayed on the 1 atm Fe-C phase diagram. At 1 atm, solid metal and liquid metal can coexist at temperatures greater than 1153 °C, while at 5 GPa, we find that the Fe- Fe_3C eutectic occurs at a temperature between 1200 and 1250 °C. This slight increase in eutectic temperature with increasing pressure is consistent with the experiments of Hirayama et al. (1993), which were conducted at 4.5, 6.8, and 12 GPa and suggested an increase of about 7 °C/GPa.

At 1 atm, Fe_3C and liquid metal do not stably coexist (Okamoto, 1990), but at 5 GPa they do. At 1 atm, the eutectic point occurs at a composition of 4.3 wt% C. In our 5 GPa experiments, we observe the eutectic composition to potentially be at a slightly higher C composition of near 4.7 wt%. We selected a C content of 4.7 wt% because our five runs conducted at 1250 °C have a range of measured C contents from 3.8 to 4.6 wt% C, and the eutectic composition must have a higher C content than these runs. Run #A417 at 1300 °C has Fe_3C coexisting with a liquid with 4.9 wt% C, requiring the eutectic composition to have a C composition lower than this value. Thus, to be consistent with the results from our experiments, a eutectic composition of 4.7 wt% C was chosen. However, it should be noted that given the uncertainties in our C measurements, we could not meaningfully distinguish between C contents as similar as 4.3 and 4.7 wt%. Hirayama et al. (1993) also suggested a small increase in the C content of the eutectic composition with increasing pressure. In their study, Hirayama et al. (1993) observed the phases created under different temperatures, pressures, and starting Fe and C compositions but did not measure the final C contents of the phases in their run products, limiting the constraints they could place on the exact eutectic composition.

In Fig. 2B, we compare our experimentally determined phases to those of the calculated 5 GPa Fe-C phase diagram presented in Wood (1993). We find significant discrepancies between our experimental results and those predicted by the calculated 5 GPa phase diagram. From our experiments, we place the Fe- Fe_3C eutectic at a temperature between 1200 and 1250 °C and at a composition of around 4.7 wt% C. In contrast, Wood (1993) suggested that the Fe- Fe_3C eutectic at 5 GPa occurs at slightly over 1300 °C and at 3.2 wt% C. The difference in the C composition of the eutectic is of particular importance. In his study, Wood (1993) suggested that the eutectic composition shifts to lower C contents as the pressure increases. At pressures applicable to Earth's outer core, Wood (1993) suggested that the Fe- Fe_3C eutectic would lie at a C content of only 0.25 wt%. The shifting of the eutectic composition

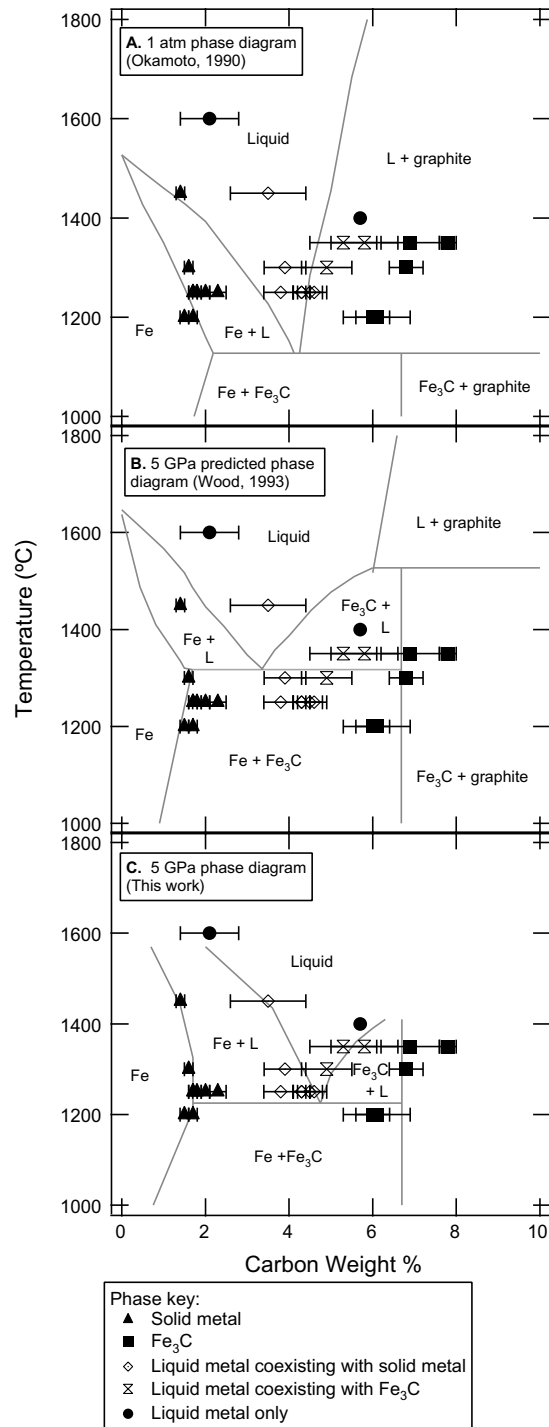


Fig. 2. Our experimental results are compared to the (A) 1 atm Fe-C phase diagram (Okamoto, 1990) and (B) a predicted 5 GPa Fe-C phase diagram (Wood, 1993). (C) Phase boundaries consistent with our experimental runs at 5 GPa are drawn. (For simplicity, the body-centered cubic δ solid phase of Fe is neglected in the phase diagrams.)

to lower C compositions is a fundamental point that Wood (1993) used to suggest that the first solid phase to crystallize in Earth's core is not Fe metal but Fe_3C . However, our

experimental results suggest that increasing pressure does not result in a shift of the eutectic composition to lower C contents. Thus, our 5 GPa experiments do not support the prediction of Wood (1993) that the eutectic composition shifts to lower C contents with increasing pressure or the reasoning that led to the conclusion that the inner core is composed of Fe₃C.

In Fig. 2C, we present a 5 GPa phase diagram consistent with our experimental run products. Our experimental results are in good agreement with those of Hirayama et al. (1993) and the more recent work of Fei et al. (2007). In their study, Fei et al. (2007) examined the Fe–C phase diagram at a variety of pressures, ranging from 5 to 25 GPa. At 5 GPa, Fei et al. (2007) report that the Fe–Fe₃C eutectic occurs between 1240 and 1250 °C, entirely in agreement with our data that suggest a eutectic temperature between 1200 and 1250 °C. Fei et al. (2007) also report that the eutectic composition is relatively insensitive to pressure in their study. We observe a slight increase in the eutectic C content, from 4.3 wt% C at 1 atm to 4.7 wt% C at 5 GPa. However, given the uncertainty in our C measurements, the difference between 4.3 and 4.7 wt% C is not significant. Of significance is that we do not observe the predicted decrease of the C content of the eutectic to 3.2 wt% C at 5 GPa as predicted by Wood (1993). Fei et al. (2007) also do not observe the C content of the eutectic composition shifting to lower values with increasing pressure.

3.2. Solid metal/liquid metal partitioning

Table 2 provides the compositional data for four solid metal/liquid metal partitioning experiments conducted at 1250 °C with a starting bulk C composition of 3 wt%. Errors in Table 2 are twice the standard deviation of the mean from multiple analyses. Table 2 also lists calculated values for D, the solid metal/liquid metal partition coefficient, for each trace element, determined as the weight ratio.

The four experiments at 1250 °C had varying run durations to evaluate the time needed to reach equilibrium. The partitioning results from this time series of experiments are plotted in Fig. 3. All of the 17 elements shown in Fig. 3 display consistent partitioning behavior that is independent of run durations from 30 min to over 6 h. While solid metal/liquid metal experiments conducted at 1 atm result in larger run products and are typically run for durations of days to ensure equilibrium (Malvin et al., 1986; Chabot et al., 2006), the time-series results of this study strongly support the hypothesis that solid metal/liquid metal equilibrium was achieved in this system in a time of less than 30 min.

Additionally, Fig. 3 compares the solid metal/liquid metal partitioning behavior of elements at 5 GPa to previously determined partitioning values at 1 atm (Chabot et al., 2006). The C content of the metallic liquid is known to have a significant effect on the partitioning behavior of many trace elements (Chabot et al., 2006), and thus the comparison between our 5 GPa and the previous 1 atm results must be made at the same C content. The average measured C content of the liquid of the four runs from the time series is 4.3 wt% C; the measured range is from 3.8 to 4.6 wt% C. However, as discussed in the previous section, we may

have a background contribution of C in our measurements of up to 0.8 wt%. Thus, conservatively, we compare our 5 GPa partitioning results to the values determined at 1 atm with C contents that ranged from 3 to 4.6 wt% C. This range of partitioning values at 1 atm is shown in Fig. 3 as a gray shaded region for each element for which such data are available. In general, there is very good agreement between our partitioning results at 5 GPa and those determined at 1 atm. This suggests that any effect of pressure on the solid metal/liquid metal partitioning behaviors of these elements in the Fe–C system between 1 atm to 5 GPa is relatively minor.

Even given the conservative and large range of C contents to which we compared our partitioning values, D(Ir) and D(Os) (Fig. 3m and n, respectively) at 5 GPa are at the lower limits of the 1 atm range, which corresponds to 3 wt% C. In contrast, D(As) (Fig. 3b) at 5 GPa is consistent with 1 atm partitioning at the high end of the C content range of 4.6 wt% C. Thus, if a single C content rather than a range of C contents was used for the comparison, it would not be possible to have agreement between the 5 GPa and 1 atm results for all three elements of Ir, Os, and As. Higher pressure experiments would be needed to constrain more precisely the pressure dependence of the partition coefficients.

The 1 atm study of Chabot et al. (2006) did not include Mo. Our experimental results suggest that Mo, like Cr, Re, and W (Chabot et al., 2006), is anthracophile (C-loving) and has a decrease in the solid metal/liquid metal partition coefficient with increasing C content of the metallic liquid. In the Fe–Ni–S system, with a S content of 9 wt%, Liu and Fleet (2001) report a solid metal/liquid metal partition coefficient for Mo of 1.0. Our Fe–C results plotted in Fig. 3 show D(Mo) with a value of 0.25, which is considerably lower than the value in the 9 wt% S system, suggesting a decrease in the partition coefficient due to the presence of C.

3.3. Fe₃C/liquid metal partitioning

The results of trace element partitioning between liquid metal and Fe₃C are given in Table 3. Errors are twice the standard error of the mean of multiple analyses. Two experiments at 1350 °C with a starting C content of 6 wt% were conducted for different durations of 37 min and just over 3 h. The good agreement between the partitioning values obtained in these two runs suggests that equilibrium was obtained in less than 37 min for this system.

Fig. 4A plots the Fe₃C/liquid metal partition coefficients from the two experiments in order of increasing atomic number. In these runs, the liquid metal has a C content of about 5.5 wt% C. For the 14 elements examined, all of the Fe₃C/liquid metal partitioning values are less than one, showing a preference for the C-bearing liquid metal phase over the solid Fe₃C phase. The anthracophile elements of Mo, W, and Re (Chabot et al., 2006) exhibit some of the highest Fe₃C/liquid metal partition coefficients of the set of elements; however, elements without anthracophile tendencies, such as Co, Ga, Ru, and Os, have equally high partitioning values, as shown in Fig. 4A. Both phases, between which the elements are partitioning, are C-rich, and

Table 2

Composition of run products at 5 GPa with solid metal and liquid metal

Run #	A174	A168	A177	A176
Temperature (°C)	1250	1250	1250	1250
Duration (min)	30	121	197	375
<i>Solid metal</i>				
Fe (wt%)	97.0 ± 0.6	99.0 ± 1.1	86.0 ± 0.1	97.4 ± 1.6
Ni (wt%)			14.1 ± 0.3	
C (wt%)	2.3 ± 0.2	2.0 ± 0.1	1.8 ± 0.1	1.7 ± 0.1
Ag (ppm)	100 ± 8	90 ± 8	70 ± 3	80 ± 3
As (ppm)	100 ± 3	90 ± 5	80 ± 4	100 ± 5
Au (ppm)	260 ± 14	200 ± 8	200 ± 7	200 ± 12
Bi (ppm)	6.4 ± 0.4	11 ± 1	12.5 ± 0.6	22.7 ± 1.1
Co (ppm)	170 ± 7	170 ± 20	370 ± 20	390 ± 14
Cu (ppm)	170 ± 10	990 ± 40	90 ± 11	380 ± 9
Ga (ppm)	210 ± 30	150 ± 13	110 ± 7	170 ± 10
Ge (ppm)	210 ± 11	20 ± 9	240 ± 14	250 ± 12
Ir (ppm)	620 ± 60	510 ± 80	370 ± 40	500 ± 50
Mo (ppm)	50 ± 4	80 ± 3	60 ± 6	50 ± 3
Os (ppm)	400 ± 40	260 ± 30	180 ± 9	330 ± 20
Pb (ppm)	15 ± 2	11.4 ± 1.1	13.4 ± 0.9	12 ± 2
Pd (ppm)	270 ± 30	230 ± 13	210 ± 60	240 ± 12
Pt (ppm)	360 ± 30	270 ± 30	190 ± 14	330 ± 30
Ru (ppm)	330 ± 20	280 ± 12	210 ± 12	390 ± 13
Sb (ppm)	70 ± 2	340 ± 20	140 ± 9	80 ± 3
W (ppm)	50 ± 2	60 ± 3	50 ± 5	80 ± 4
<i>Liquid metal</i>				
Fe (wt%)	94.6 ± 1.5	97.0 ± 0.7	87.3 ± 0.5	96.4 ± 1.5
Ni (wt%)			9.9 ± 0.2	
C (wt%)	4.6 ± 0.2	4.5 ± 0.4	4.3 ± 0.2	3.8 ± 0.4
Ag (ppm)	150 ± 2	150 ± 2	98.6 ± 1.4	150 ± 2
As (ppm)	132.3 ± 1.4	150 ± 3	100 ± 2	150 ± 3
Au (ppm)	180 ± 2	170 ± 3	130 ± 3	160 ± 2
Bi (ppm)	70 ± 3	140 ± 2	130 ± 2	290 ± 3
Co (ppm)	140 ± 3	140 ± 2	320 ± 3	330 ± 3
Cu (ppm)	120 ± 2	740 ± 4	60 ± 4	290 ± 3
Ga (ppm)	90 ± 2	70 ± 5	40 ± 3	90 ± 7
Ge (ppm)	110 ± 3	130 ± 8	110 ± 3	140 ± 3
Ir (ppm)	160 ± 7	130 ± 4	100 ± 3	130 ± 5
Mo (ppm)	200 ± 2	300 ± 3	250 ± 1	190 ± 3
Os (ppm)	140 ± 8	90 ± 9	60 ± 3	110 ± 4
Pb (ppm)	90 ± 3	80 ± 2	80 ± 2	80 ± 3
Pd (ppm)	150 ± 3	142.6 ± 1.2	100 ± 2	160 ± 3
Pt (ppm)	110 ± 6	90 ± 4	60 ± 3	110 ± 5
Ru (ppm)	190 ± 6	160 ± 3	130 ± 2	220 ± 2
Sb (ppm)	83.3 ± 1.4	460 ± 2	150 ± 1	120 ± 2
W (ppm)	140 ± 2	170 ± 3	170 ± 2	200 ± 3
<i>D(SM/LM)^a</i>				
Ag	0.67 ± 0.06	0.58 ± 0.06	0.68 ± 0.04	0.53 ± 0.03
As	0.72 ± 0.03	0.63 ± 0.05	0.81 ± 0.05	0.69 ± 0.05
Au	1.4 ± 0.1	1.39 ± 0.09	1.71 ± 0.11	1.3 ± 0.1
Bi	0.10 ± 0.01	0.08 ± 0.01	0.10 ± 0.01	0.08 ± 0.01
Co	1.2 ± 0.1	1.24 ± 0.13	1.2 ± 0.1	1.2 ± 0.1
Cu	1.41 ± 0.11	1.32 ± 0.11	1.6 ± 0.2	1.3 ± 0.1
Ga	2.4 ± 0.3	2.2 ± 0.3	2.6 ± 0.2	1.8 ± 0.3
Ge	1.86 ± 0.14	1.7 ± 0.3	2.1 ± 0.2	1.75 ± 0.12
Ir	3.9 ± 0.6	4.1 ± 0.7	3.9 ± 0.4	3.7 ± 0.5
Mo	0.25 ± 0.02	0.26 ± 0.02	0.22 ± 0.03	0.27 ± 0.02
Os	2.8 ± 0.5	2.9 ± 0.6	2.9 ± 0.2	2.9 ± 0.3
Pb	0.17 ± 0.02	0.15 ± 0.01	0.17 ± 0.01	0.14 ± 0.03
Pd	1.8 ± 0.2	1.6 ± 0.1	2.2 ± 0.6	1.47 ± 0.12
Pt	3.1 ± 0.4	3.2 ± 0.4	3.4 ± 0.3	2.9 ± 0.4
Ru	1.7 ± 0.2	1.78 ± 0.13	1.68 ± 0.12	1.8 ± 0.1
Sb	0.80 ± 0.03	0.74 ± 0.04	0.91 ± 0.06	0.70 ± 0.04
W	0.34 ± 0.02	0.36 ± 0.03	0.32 ± 0.03	0.37 ± 0.03

Errors are twice the standard deviation of the mean.

^a D(SM/LM), D(solid metal/liquid metal).

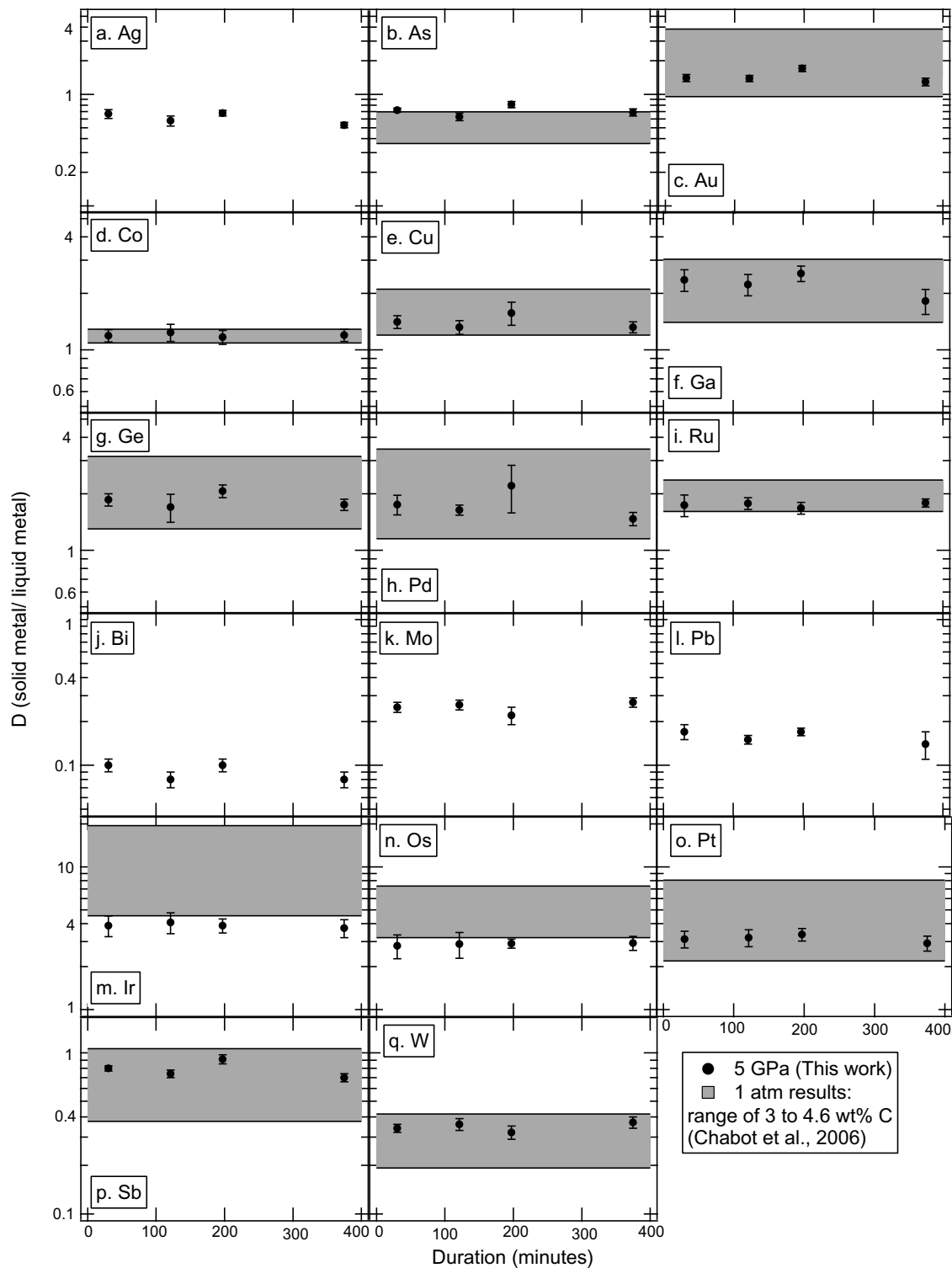


Fig. 3. Solid metal/liquid metal partition coefficients are plotted as a function of the run duration. For all of the 17 elements shown, the partition coefficients are constant over the range of run durations, indicating that equilibrium partitioning behavior was achieved in less than 30 min. The partitioning values measured at 5 GPa also show general agreement with values determined at 1 atm with similar C contents of the metallic liquid (Chabot et al., 2006). (Elements are ordered to allow sharing of the y -axis and to enable the results from all 17 elements to be displayed on one figure.)

consequently the amount of C may not be a dominant influence on governing partitioning in this system.

Fig. 4A also shows the divisions of the elements into their different periods. Within a given period of elements,

Table 3

Composition of run products at 5 GPa with liquid metal and Fe ₃ C		
Run #	A421	A423
Temperature (°C)	1350	1350
Duration (min)	37	181
<i>Fe₃C</i>		
Fe (wt%)	93.7 ± 1.2	94.1 ± 0.7
C (wt%)	6.9 ± 0.7	7.8 ± 0.2
Ag (ppm)	4 ± 2	—
As (ppm)	2.0 ± 0.8	—
Au (ppm)	3.7 ± 1.2	—
Co (ppm)	—	80 ± 6
Cu (ppm)	6 ± 2	40 ± 10
Ga (ppm)	—	10 ± 6
Ir (ppm)	34 ± 20	5 ± 2
Mo (ppm)	60 ± 30	90 ± 20
Os (ppm)	40 ± 20	20 ± 4
Pd (ppm)	11 ± 2	4 ± 2
Pt (ppm)	8 ± 4	—
Re(ppm)	—	34 ± 12
Ru (ppm)	80 ± 30	45 ± 14
W (ppm)	61 ± 8	42 ± 8
<i>Liquid metal</i>		
Fe (wt%)	94.1 ± 1.4	95.9 ± 0.7
C (wt%)	5.8 ± 0.8	5.3 ± 0.8
Ag (ppm)	150 ± 6	—
As (ppm)	200 ± 12	—
Au (ppm)	230 ± 14	—
Co (ppm)	—	120 ± 1
Cu (ppm)	30 ± 4	280 ± 20
Ga (ppm)	—	28.2 ± 1.4
Ir (ppm)	270 ± 14	130 ± 8
Mo (ppm)	120 ± 20	200 ± 12
Os(ppm)	110 ± 14	150 ± 6
Pd (ppm)	170 ± 10	110 ± 8
Pt (ppm)	210 ± 14	—
Re(ppm)	—	90 ± 4
Ru (ppm)	150 ± 8	150 ± 4
W (ppm)	130 ± 4	80 ± 2
<i>D (Fe₃C/Liquid metal)</i>		
Ag	0.02 ± 0.01	—
As	0.010 ± 0.004	—
Au	0.02 ± 0.01	—
Co	—	0.64 ± 0.05
Cu	0.18 ± 0.06	0.14 ± 0.04
Ga	—	0.36 ± 0.22
Ir	0.13 ± 0.06	0.04 ± 0.02
Mo	0.29 ± 0.16	0.75 ± 0.19
Os	0.35 ± 0.17	0.13 ± 0.03
Pd	0.06 ± 0.01	0.04 ± 0.02
Pt	0.04 ± 0.02	—
Re	—	0.39 ± 0.14
Ru	0.49 ± 0.22	0.31 ± 0.10
W	0.47 ± 0.06	0.56 ± 0.11

Errors are twice the standard deviation of the mean.

there is a decrease in the Fe₃C/liquid metal partitioning value moving from left to right across the period. In our dataset, this decreasing trend is particularly striking for the elements in Period 6, with a steady decrease in the Fe₃C/liquid metal value from W to Au. An element's atomic radius also decreases from left to right across a given

period, but we do not observe a simple relationship between an element's atomic radius and its Fe₃C/liquid metal partitioning value, as shown in Fig. 4B. Within a given period, the element with the larger atomic radius has a higher Fe₃C/liquid metal value, but elements such as Co and W, which have very different atomic radii, have similar Fe₃C/liquid metal partitioning values. Thus, size alone is not controlling an element's Fe₃C/liquid metal partitioning behavior, but the behavior does exhibit periodic trends.

The distribution of trace elements in iron meteorites between cohenite, (Fe,Ni)₃C, and kamacite metal has been measured by laser ablation ICP-MS studies (Campbell and Humayun, 1999a; McDonough et al., 1999; Gangopadhyay et al., 2006). To compare the partitioning behaviors from our experiments to those observed in iron meteorites, we need Fe₃C/solid metal partition coefficients. However, our experiments that contain coexisting Fe₃C and solid metal are subsolidus runs, making it more difficult to reach chemical equilibrium for trace element partitioning. As an estimate of Fe₃C/solid metal behavior, we divided our Fe₃C/liquid metal partition coefficients from Table 3 by our solid metal/liquid metal partition coefficients from Table 2. The two liquid metal phases from the experiments in Tables 2 and 3 have different C contents, 4.3 and 5.5 wt%, respectively. Thus, dividing the two partition coefficients is an imperfect way to get the Fe₃C/solid metal partition coefficient, but it does provide an estimate of the expected partitioning behavior. Fig. 5 compares our estimated Fe₃C/solid metal partition coefficients to cohenite/kamacite values measured in the iron meteorite Odessa (Campbell and Humayun, 1999a; Gangopadhyay et al., 2006). Measurements of cohenite/kamacite ratios in the iron meteorite Canyon Diablo give similar values to Odessa (McDonough et al., 1999; Gangopadhyay et al., 2006). Given the imperfections in our method of estimating a Fe₃C/solid metal partitioning value, the lack of Ni in our study, and the large difference in equilibration temperatures, there is agreement between our experimental results and the cohenite/kamacite behavior observed in iron meteorites.

Our 5 GPa Fe-C phase diagram results discussed previously do not agree with the predicted phase diagram of Wood (1993) and consequently do not support Wood's reasoning that Earth's inner core is composed of Fe₃C. Interestingly, more recent results by Fei et al. (2008) suggest that phase relations in the Fe-S-C system may indeed result in Earth's inner core being composed of a Fe carbide phase for very different reasons than suggested by Wood (1993). The preliminary results of Fei et al. (2008) report that below 5 GPa, Fe₃C may be the first solid to form in the Fe-S-C system but above 5 GPa, Fe₇C₃ may become stable. Of course, both experimental studies require considerable extrapolation to be applied to Earth's inner core-outer core pressure of 330 GPa, which is reason for caution and should be properly noted. Moreover, a Fe₃C inner core would require an outer core that is less dense than Fe₃C, unlike the melts produced in this study. As the identity of Earth's inner core continues to be an area of active research, our new experiments in this system allow us to cautiously explore, for the first time, partitioning in the Fe₃C/liquid metal system and examine the possible elemental

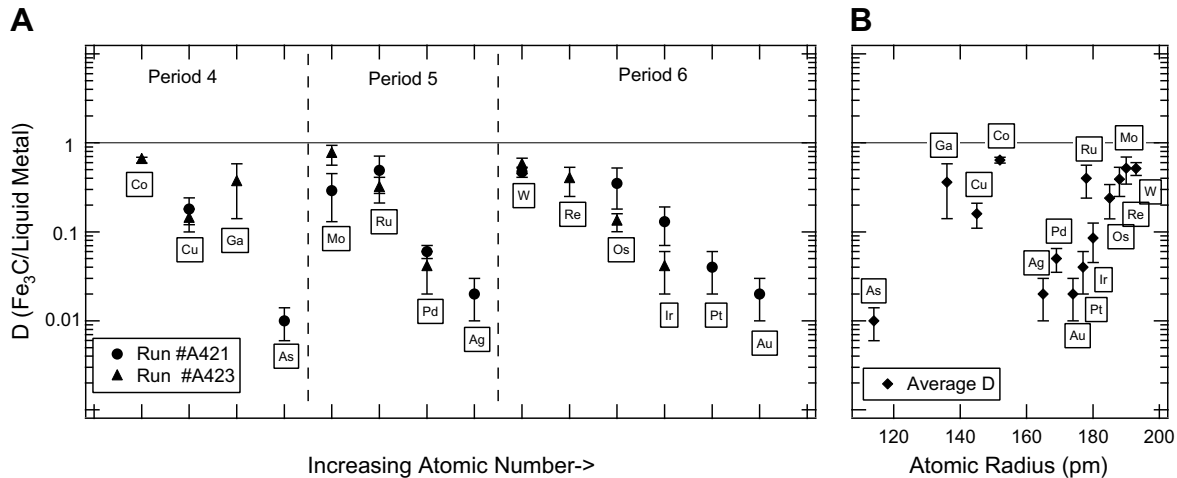


Fig. 4. (A) Fe_3C /liquid metal partitioning values for 14 trace elements are plotted in order of increasing atomic number. All elements have Fe_3C /liquid metal partitioning values less than one, indicating a preference for the C-bearing metallic liquid over the solid Fe_3C phase. Moving across a given period, a decreasing Fe_3C /liquid metal trend is observed, but (B) the decreasing trend is not a simple function of atomic radius size. (Atomic radii from Clementi et al., 1967).

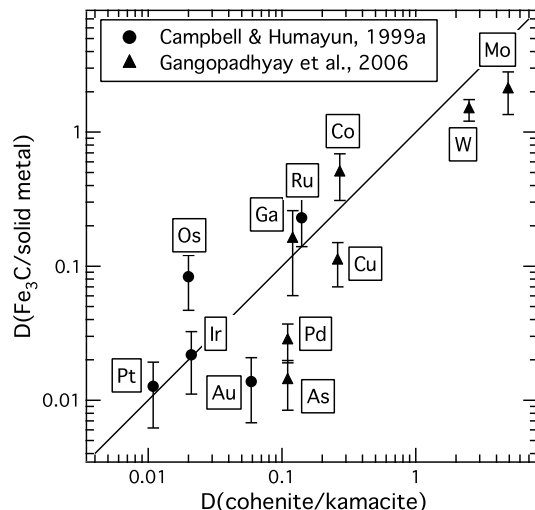


Fig. 5. Our experimental partitioning results are compared to cohenite ($(\text{Fe}, \text{Ni})_3\text{C}$)/kamacite values measured in the iron meteorite Odessa (Campbell and Humayun, 1999a; Gangopadhyay et al., 2006). There is a general correlation, shown by the 1:1 line in the figure, between the observed iron meteorite trace element partitioning behavior and that determined in this study experimentally.

fractionations that could result if Earth's core, or any planetary core, crystallized Fe_3C .

Having quantified elemental partitioning in the Fe_3C /liquid metal system at 5 GPa, we can assess the elemental fractionations that would ensue in a system crystallizing Fe_3C . We stress that, for Earth, (a) our phase relations make this scenario unlikely and (b) the experimental pressure is orders of magnitude lower than that of Earth's core. Nevertheless, because it has been suggested that fractionation of Os from Pt and Re in Earth's core may account for the Os isotopic signatures measured in some mantle plume sources (Walker et al., 1995, 1997; Brandon et al.,

1998, 1999, 2003; Puchtel et al., 2005), it is relevant to comment on whether or not the current set of experiments are consistent with such fractionations. ^{187}Re decays to ^{187}Os with a half-life of ~ 42 Ga, and ^{190}Pt decays to ^{186}Os with a half-life of ~ 489 Ga. Thus, to create an elevated, radiogenic Os isotopic signature, the source material, in this case the liquid outer core, must be enriched in both Re and Pt relative to Os in comparison to their chondritic ratios, with a Pt/Re ratio ~ 80 , and that enrichment must have occurred relatively early in solar system history (Puchtel et al., 2005).

For Pt and Os, Fe_3C /liquid metal partition coefficients differ by a factor of 6 in our experiments, with a value of 0.04 for Pt and a much higher average value for Os of 0.24. The higher Fe_3C /liquid metal value for Os indicates that Os would be enriched in an inner core of Fe_3C relative to Pt. However, for a model inner core with a comparable mass fraction as that of Earth, the inner core represents only 5.5% of the bulk core by mass, and the experimental data imply an increase in the Pt/Os ratio of the liquid outer core of about 1%. Application of this simple model to Earth, albeit with the understanding of the differences in pressure conditions, suggests that this effect is too small to account for the Os isotopic signatures observed in mantle plumes (Brandon et al., 1999, 2003; Puchtel et al., 2005), which require over a factor of two change in the Pt/Os ratio of the outer core.

Rhenium and Os have comparable Fe_3C /liquid metal partitioning values in our experiments. Similar partitioning behaviors would not create fractionations between Re and Os. Furthermore, the Fe_3C /liquid metal partitioning value for Re was determined in only one of our experiments and has a value of 0.39. The average Fe_3C /liquid metal partitioning value for Os in our experiments is 0.24. If the Fe_3C /liquid metal partitioning value for Re is larger than that for Os, Re will be enriched relative to Os in a solid inner core composed of Fe_3C and Os would be enriched relative to Re in the liquid outer core. These enrichments are

opposite to those needed to produce an elevated Os isotopic signature in Earth's outer core.

Thus, based on our 5 GPa experiments, our results suggest that if the presence of C in Earth's core did stabilize the formation of Fe₃C, an inner core of Fe₃C would not significantly enrich the liquid outer core in Pt and Re relative to Os. However, even if C is a significant light element in Earth's core, it is likely not the only light element but rather is accompanied by other light elements, such as S, Si, O, P, or H. Partitioning data from systems with multiple light elements and at higher pressures and temperatures are needed to conduct a more thorough exploration of the partitioning behaviors of Pt, Re, and Os between Earth's inner and outer cores.

4. CONCLUSIONS

In this experimental study, we established the Fe-rich portion of the Fe-C phase diagram at 5 GPa. Our experimentally determined Fe-C phase diagram differs considerably from the one predicted by Wood (1993) at 5 GPa. In particular, we do not find that the Fe-Fe₃C eutectic composition shifts to lower C contents at higher pressures, which is a central argument in the reasoning of Wood (1993) that the inner core may be composed of Fe₃C. Thus, even if C is present in Earth's core, our work does not support Wood's reasoning that Earth's inner core is composed of Fe₃C.

Our new partitioning data suggest that the effect of pressure on solid metal/liquid metal partitioning behaviors in the Fe-C system between 1 atm and 5 GPa is relatively minor. Our experimental results involving Fe₃C show good agreement with cohenite/kamacite behavior observed in iron meteorites. In addition, our experiments with coexisting Fe₃C and liquid metal allow us to cautiously explore, for the first time, the elemental fractionations an inner core of Fe₃C could cause, with specific focus on the elements of Pt, Re, and Os. We find that an inner core of Fe₃C would fail to sufficiently enrich Pt and Re relative to Os in the liquid outer core, which would be needed to generate an elevated Os isotopic signature consistent with that measured in mantle plume sources.

ACKNOWLEDGMENTS

This work was supported by a number of research grants: NASA grants NNG06GI13G to N.L. Chabot, NNG04GG17G to W.F. McDonough, NNG05GB81G to M. Humayun, and NSF Grant No. EAR-0600140 to A.J. Campbell. We appreciate comments from two anonymous reviewers and associate editor A.D. Brandon, which led to improvements in this manuscript.

REFERENCES

- Achterbergh E. V., Ryan C. G., Jackson S. E. and Griffin W. L. (2001) Appendix 3: Data reduction software for LA-ICP-MS. In *Laser Ablation-ICP-MS in the Earth Sciences*, vol. 29 (ed. P. Sylvester). Mineralogical Association of Canada, Short Course Series, 243 pp.
- Agee C. B., Li J., Shannon M. C. and Circone S. (1995) Pressure-temperature phase diagram for the Allende meteorite. *J. Geophys. Res.* **100**, 17725–17740.
- Anderson O. L. and Isaak D. G. (2002) Another look at the core density deficit of Earth's outer core. *Phys. Earth Planet. Int.* **131**, 19–27.
- Brandon A. D., Walker R. J., Morgan J. W., Norman M. D. and Prichard H. M. (1998) Coupled ¹⁸⁶Os and ¹⁸⁷Os evidence for core–mantle interaction. *Science* **280**, 1570–1573.
- Brandon A. D., Norman M. D., Walker R. J. and Morgan J. W. (1999) ¹⁸⁶Os–¹⁸⁷Os systematics of Hawaiian picrites. *Earth. Planet. Sci. Lett.* **174**, 25–42.
- Brandon A. D., Walker R. J., Puchtel I. S., Becker H., Humayun M. and Revillon S. (2003) ¹⁸⁶Os–¹⁸⁷Os systematics of Gorgona Island komatiites: implications for early growth of the inner core. *Earth Planet. Sci. Lett.* **206**, 411–426.
- Buchwald V. F. (1975). *Handbook of Iron Meteorites*, vol. 1. University of California Press, Berkeley.
- Campbell A. J. and Humayun M. (1999a) Microanalysis of platinum group elements in iron meteorites using laser ablation ICP-MS. *Lunar and Planet. Sci. XXX*. Lunar and Planetary Institute, Houston (CD-ROM). #1974 (abstr.).
- Campbell A. J. and Humayun M. (1999b) Trace element microanalysis in iron meteorites by laser ablation ICPMS. *Anal. Chem.* **71**, 939–946.
- Campbell A. J., Humayun M. and Weisberg M. K. (2002) Siderophile element constraints on the formation of metal in the metal-rich chondrites Bencubbin, Weatherford, and Gujba. *Geochim. Cosmochim. Acta* **66**, 647–660.
- Chabot N. L. (2004) Sulfur contents of the parental metallic cores of magmatic iron meteorites. *Geochim. Cosmochim. Acta* **68**, 3607–3618.
- Chabot N. L., Campbell A. J., Jones J. H., Humayun M. and Agee C. B. (2003) An experimental test of Henry's Law in solid metal–liquid metal systems with implications for iron meteorites. *Meteorit. Planet. Sci.* **38**, 181–196.
- Chabot N. L., Campbell A. J., Jones J. H., Humayun M. and Lauer H. V. (2006) The influence of carbon on trace element partitioning behavior. *Geochim. Cosmochim. Acta* **70**, 1322–1335.
- Chabot N. L., Saslow S. A., McDonough W. F. and McCoy T. J. (2007) The effect of Ni on element partitioning during iron meteorite crystallization. *Meteorit. Planet. Sci.* **42**, 1735–1750.
- Clementi E., Raimondi D. L. and Reinhardt W. P. (1967) Atomic screening constants from SCF functions. II. Atoms with 37 to 86 electrons. *J. Chem. Phys.* **47**, 1300–1307.
- Fei Y., Wang Y. and Deng L. (2007) Melting relations in the Fe–S system at high pressure: implications for the chemistry in the cores of the terrestrial planets. *Lunar and Planetary Science Conference XXXVIII*, 1231.
- Fei Y., Deng L. and Corgne A. (2008) Effect of carbon and sulfur on iron melting at high pressure: implications for composition and evolution of the terrestrial planet cores. *Lunar and Planetary Science Conference XXXIX*, 1687.
- Gangopadhyay A., Humayun M. and Goddard R. E. (2006) The partitioning of siderophile elements between kamacite and cohenite. *Lunar and Planetary Science Conference XXXVII*. Lunar and Planetary Institute, Houston (CD-ROM). #1456 (abstr.).
- Haack H. and Scott E. R. D. (1993) Chemical fractionations in Group IIIAB iron meteorites: origin by dendritic crystallization of an asteroidal core. *Geochim. Cosmochim. Acta* **57**, 3457–3472.
- Hillgren V. J., Gessmann C. K. and Li J. (2000) An experimental perspective on the light element in Earth's core. In *Origin of the Earth and Moon* (eds. R. M. Canup and K. Righter). The University of Arizona Press, Tucson, pp. 245–263.
- Hirayama Y., Fujii T. and Kurita K. (1993) The melting relation of the system, iron and carbon at high pressure and its bearing on the early stage of the Earth. *Geophys. Res. Lett.* **20**, 2095–2098.

- Humayun M. and Clayton R. N. (1995) Potassium isotope cosmochemistry: genetic implications of volatile element depletion. *Geochim. Cosmochim. Acta* **59**, 2131–2148.
- Jepcoat A. and Olson P. (1987) Is the inner core of the Earth pure iron? *Nature* **325**, 332–335.
- Li J., Mao H. K., Fei Y., Gregory E., Eremets M. and Zha C. S. (2002) Compression of Fe_3C to 30 GPa at room temperature. *Phys. Chem. Miner.* **29**, 166–169.
- Liu M. and Fleet M. E. (2001) Partitioning of siderophile elements (W, Mo, As, Ag, Ge, Ga, and Sn) and Si in the Fe–S system and their fractionation in iron meteorites. *Geochim. Cosmochim. Acta* **65**, 671–682.
- Lodders K. (2003) Solar system abundances and condensation temperatures of the elements. *Astrophys. J.* **591**, 1220–1247.
- Malvin D. J., Jones J. H. and Drake M. J. (1986) Experimental investigations of trace element fractionation in iron meteorites. III: Elemental partitioning in the system Fe–Ni–S–P. *Geochim. Cosmochim. Acta* **50**, 1221–1231.
- McDonough W. F., Horn I., Lange D. and Rudnick R. L. (1999) Distribution of platinum group elements between phases in iron meteorites. *Lunar and Planetary Science Conference XXX*, 2062.
- McDonough W. F. (2003) Compositional model for the Earth's core. In *The Mantle and Core*, vol. 2 (ed. R. W. Carlson) (eds. H. D. Holland and K. K. Turekian). Treatise on Geochemistry. Elsevier-Pergamon, Oxford, pp. 547–568.
- Okamoto H. (1990) C–Fe (Carbon–Iron). In *Binary Alloy Phase Diagrams*, second ed., vol. 1 (ed. T. B. Massalski). ASM International, pp. 842–848.
- Puchtel I. S., Brandon A. D., Humayun M. and Walker R. J. (2005) Evidence for the early differentiation of the core from Pt–Re–Os isotope systematics of 2.8 Ga komatiites. *Earth Planet. Sci. Lett.* **237**, 118–134.
- Scott E. R. D. (1972) Chemical fractionation in iron meteorites and its interpretation. *Geochim. Cosmochim. Acta* **36**, 1205–1236.
- Scott H. P., Williams Q. and Knittle E. (2001) Stability and equation of state of Fe_3C to 73 GPa: implications for carbon in the Earth's core. *Geophys. Res. Lett.* **28**, 1875–1878.
- Vocadlo L., Brodholt J., Dobson D. P., Knight K. S., Marshall W. G., Price G. D. and Wood I. G. (2002) The effect of ferromagnetism on the equation of state of Fe_3C studied by first-principles calculations. *Earth Planet. Sci. Lett.* **203**, 567–575.
- Walker R. J., Morgan J. W. and Horan M. F. (1995) Osmium-187 enrichment in some plumes: evidence for core–mantle interaction? *Science* **269**, 819–822.
- Walker R. J., Morgan J. W., Beary E. S., Smolar M. I., Czamanske G. K. and Horan M. F. (1997) Applications of the ^{190}Pt – ^{186}Os isotope system to geochemistry and cosmochemistry. *Geochim. Cosmochim. Acta* **61**, 4799–4807.
- Wood B. J. (1993) Carbon in the core. *Earth Planet. Sci. Lett.* **117**, 593–607.
- Wood I. G., Vocadlo L., Knight K. S., Dobson D. P., Marshall W. G., Price G. D. and Brodholt J. (2004) Thermal expansion and crystal structure of cementite, Fe_3C , between 4 and 600 K determined by time-of-flight neutron powder diffraction. *J. Appl. Crystallogr.* **37**, 82–90.

Associate editor: Alan D. Brandon